

**PCCP****Exchange Equilibria of Carboxylate-Terminated Ligands at  
PbS Nanocrystal Surfaces**

Journal:	<i>Physical Chemistry Chemical Physics</i>
Manuscript ID	CP-ART-07-2018-004275.R1
Article Type:	Paper
Date Submitted by the Author:	27-Aug-2018
Complete List of Authors:	Kessler, Melody; University of North Carolina, Chemistry Starr, Hannah; University of North Carolina, Chemistry Knauf, Robin; University of North Carolina, Chemistry Rountree, Kelley; University of North Carolina, Chemistry Dempsey, Jillian; University of North Carolina, Chemistry

SCHOLARONE™  
Manuscripts



Journal Name

ARTICLE

## Exchange Equilibria of Carboxylate-Terminated Ligands at PbS Nanocrystal Surfaces

Melody L. Kessler,<sup>‡</sup> Hannah E. Starr,<sup>‡</sup> Robin R. Knauf, Kelley J. Rountree, and Jillian L. Dempsey\*Received 00th January 20xx,  
Accepted 00th January 20xx

DOI: 10.1039/x0xx00000x

www.rsc.org/

Ligand exchange reactions are commonly used to alter the surface chemistry of metal chalcogenide quantum dots; however, a lack of quantifiable data for these processes limits the rational functionalization of nanomaterials. Here, we quantify the X-type ligand exchange reaction between carboxylate-terminated ligands on PbS quantum dots via <sup>1</sup>H NMR spectroscopy. Using spectroscopic handles of both the native and exchange ligand, bound and free forms of each have been quantified as a function of exchange ligand concentration. We find that the equilibrium constants for the reaction between oleate-capped PbS quantum dots and undec-10-enoic acid are  $2.23 \pm 0.50$  and  $2.14 \pm 0.42$  for sets of nanocrystals prepared by two different synthetic methods. X-ray photoelectron, absorbance, and emission spectroscopies indicate that the carboxylate exchange reaction does not alter the lead ion coverage of the nanocrystal surface. The quantitative equilibrium constant determined herein can be used to improve control over partial ligand exchange reactions on PbS nanocrystals.

### Introduction

Widespread interest in colloidal quantum dots (QDs) arises from high optical and electronic tunability imparted by quantum confinement, a property that is advantageous for a diverse array of applications from optoelectronic devices<sup>1–3</sup> to biological probes<sup>4</sup>. QDs consist of inorganic nanocrystalline cores that are stabilized by organic capping ligands, which dictate the nucleation and growth of the nanocrystals and provide solubility in organic solvents.<sup>5</sup> The native ligands, typically long hydrocarbon chains with an anchoring group such as a carboxylate, phosphonate, or thiolate, can be exchanged with another coordinating ligand to alter solubility,<sup>6,7</sup> bridge QDs to increase inter-QD energy transfer,<sup>8</sup> or decrease nanoparticle spacing for enhanced electronic communication.<sup>9,10</sup> While such exchange reactions are regularly performed, the effect of semiconductor material, anchoring group, and ligand tail properties on the driving force for the reaction is not well-understood, hindering efforts to selectively incorporate a fraction of functionalized ligands into the ligand shell as opposed to a complete ligand exchange. At the same time, a deeper understanding of the governing mechanism(s) of ligand exchange is crucial to improve control over nanocrystal surface chemistry.

Carboxylic acids are routinely employed in QD synthesis due to long-term solution-phase stability, and are also attractive

as they undergo facile exchange with other ligands terminated with various anchoring groups. Many studies examining ligand exchange reactions have centered on exchange between native bound carboxylates and other X-type ligands<sup>11–13</sup>, but recently the existence of Z-type metal carboxylate ligands on QD surfaces has been identified and their lability demonstrated.<sup>14–16</sup> The identity of a Z-type ligand as a neutral MX<sub>2</sub> moiety, equivalently a metal cation bound to two X-type constituents, requires us to distinguish between the reactivity of native X- and Z-type ligands. Nuclear magnetic resonance (NMR) spectroscopy is a powerful tool for monitoring the surface reactions of nanocrystals, yet it alone cannot differentiate between the aforementioned types of displaced ligands. Thus, additional spectroscopic techniques must be employed to probe the reactivity of the inorganic-organic interface.

Unique spectroscopic handles for native and exchange ligands are necessary to quantify exchange reactions at the QD surface, but many of the long-chain aliphatic ligands typically used to passivate colloidal QDs have overlapping resonances for their alkyl protons in <sup>1</sup>H NMR spectra, limiting their utility for probing reactivity. However, quantification of ligand–QD and ligand chain–chain interactions has been achieved for a small number of exchange reactions employing effective native and exchange ligands, and these studies have established a measure for understanding ligand exchange on QD surfaces. For example, Kroupa et al. quantified the reaction of *trans*-2,6-difluorocinnamic acid ligands with oleate-capped PbS QDs via <sup>19</sup>F NMR spectroscopy and found that the X-type exchange equilibrium was dependent on the ligand–ligand steric and electronic interactions.<sup>17</sup> In our own lab, we recently quantified the reaction of a carboxylate-terminated aliphatic ligand, undec-10-enoic acid (UDA) (Scheme 1), with oleate-ligated CdSe

Department of Chemistry, University of North Carolina, Chapel Hill, NC, USA 27599  
3290. E-mail: dempseyj@email.unc.edu

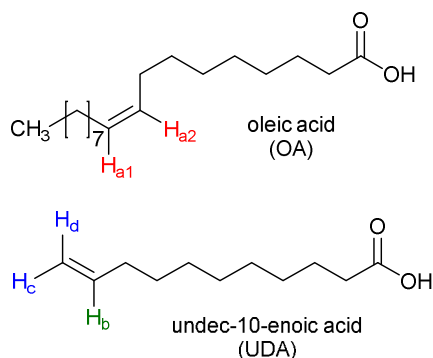
<sup>a</sup> ‡ These authors contributed equally.

Electronic Supplementary Information (ESI) available. See  
DOI: 10.1039/x0xx00000x

QDs by monitoring the alkenyl resonances of each species using  $^1\text{H}$  NMR spectroscopy.<sup>18</sup> The equilibrium constant of the identical exchange reaction on CdSe QDs was subsequently corroborated by Hens and coworkers, who further demonstrated that the X-type exchange between linear and branched carboxylic acids is dependent upon ligand sterics.<sup>19</sup> While these studies form a small library of equilibrium constants, a relative lack of quantifiable data for benchmarking the ligand exchange reactivity at QD surfaces limits our predictive power in designing functional nanomaterials.

To this extent, we have quantified the exchange reaction between carboxylate-terminated aliphatic ligands on PbS QDs prepared by two well-established synthetic procedures via  $^1\text{H}$  NMR spectroscopy. In this work, we employ UDA as an exchange ligand to gain new, quantitative information about ligand exchange reactions on PbS QDs and insight into the QD surface. In tandem with  $^1\text{H}$  NMR spectroscopy, we have utilized X-ray photoelectron, absorbance, and photoluminescence spectroscopies to probe whether Z-type ligands at the QD surface are perturbed in the carboxylate exchange reaction. By comparing with our previous work on CdSe QDs, we have begun to elucidate how ligand structure and crystal facets influence the driving force for ligand exchange reactions.

**Scheme 1** Ligands employed in this study



## Experimental

**General considerations.** Standard Schlenk line techniques were utilized to maintain an inert atmosphere during the synthesis of QDs, unless otherwise noted. Benzene-*d*<sub>6</sub> was purchased from Cambridge Isotope Laboratories and used without further purification. All other reagents were commercially available and used without further purification.

**NMR spectroscopy.**  $^1\text{H}$  NMR spectra were collected using a 600 MHz Bruker NMR spectrometer. All spectra were recorded at 25 °C with 8 scans and a relaxation delay time (*d*<sub>1</sub>) of 10 to 15 seconds to allow complete spin relaxation. The multipeak fitting function in MestreNova was used to integrate vinyl and alkenyl peaks in the  $^1\text{H}$  NMR spectra.

**X-ray photoelectron spectroscopy.** X-ray photoelectron spectroscopy (XPS) was performed using a Kratos Axis Ultra DLD X-ray photoelectron spectrometer with a monochromatic Al K $\alpha$  X-ray source. Survey and high-resolution scans were obtained with pass energies of 80 and 20 eV, respectively. All spectra were corrected to the C 1s peak at 284.6 eV.

**Transmission electron microscopy.** Transmission electron microscopic images were recorded on a JEOL 2010F-FasTEM microscope operating at 200 kV. Samples were prepared by dropping dilute solutions of nanocrystals onto a 400 mesh lacey carbon grid (Ted Pella, Inc.) and were dried overnight under vacuum at room temperature.

**Absorbance measurements.** Absorbance measurements were recorded using Cary 50 and Cary 60 UV-Visible absorbance spectrophotometers.

**Photoluminescence measurements.** Photoluminescence spectra were acquired with a PTI QuantaMaster 4SE-NIR emission spectrometer equipped with a housed 75 W xenon light source and Hamamatsu R928P PMT biased at 1100 V (1 nm step size, 10 nm bandwidth). Samples were excited at 840 nm and detected from 850 nm to 1050 nm.

**Synthesis of PbS QDs via the method of Owen (O-PbS).** PbS QDs were synthesized by modifying the method previously established by Hendricks et al.<sup>20</sup> Preparation and isolation of Pb(oleate)<sub>2</sub> was conducted under ambient conditions. Lead (II) oxide (5.05 g, 22.6 mmol) was suspended in acetonitrile (10 mL) and stirred in an ice bath for 10 min. Trifluoroacetic acid (0.35 mL, 4.48 mmol) and trifluoroacetic anhydride (3.1 mL, 22.4 mmol) were added and the resulting mixture was stirred for 30 min then warmed to room temperature. The reaction mixture was added to a solution of oleic acid (12.7 g, 45.0 mmol) and triethylamine (5.12 g, 50.6 mmol) in isopropanol (90 mL) in a round bottom flask. The mixture was stirred until a white precipitate formed and then refluxed until the precipitate dissolved, about 30 min. The mixture was cooled to room temperature then stored at -20 °C overnight. The solid was isolated via suction filtration and washed with methanol. The resulting Pb(oleate)<sub>2</sub> (13 g) was dried under vacuum and the product was stored in a desiccator.

To synthesize the QDs, Pb(oleate)<sub>2</sub> (2.94 g, 3.81 mmol) and 1-octene (50 mL) were combined in a 100 mL three-neck round bottom flask. The mixture was degassed, taking care to avoid solvent loss, and placed under a nitrogen atmosphere. Separately, *N,N*-diphenylthiourea (0.581 g, 2.54 mmol) and diglyme (1.67 mL) were combined in a two-neck pear-shaped flask in air, degassed, and placed under a nitrogen atmosphere. The Pb(oleate)<sub>2</sub> mixture was heated to 95 °C and the thiourea solution rapidly injected via syringe. The reaction mixture rapidly turned dark brown, and the flask was removed from the heating mantle after 1 min. The reaction mixture was cooled to room temperature and the solution was concentrated under vacuum. The solution was divided among six tubes and centrifuged at 8500 rpm for 10 min with acetone antisolvent. The pale brown supernatant was decanted and the precipitated QDs were resuspended in minimal (<2 mL) pentane. Acetone

(10 mL) was added and the QDs were centrifuged and resuspended for five additional cycles. PbS QDs were isolated by solvent evaporation, suspended in benzene- $d_6$ , and stored under air in the dark. The first excitonic absorbance of the O-PbS QDs was centered at 940 nm, corresponding to a diameter of 3.05 nm as determined by the sizing curve from Moreels et al.<sup>21</sup>

**Synthesis of PbS QDs via the method of Hines and Scholes (HS-PbS).** PbS QDs were synthesized following a modified version of the procedure established by Hines and Scholes.<sup>22</sup> Lead (II) oxide (0.450 g, 2 mmol), oleic acid (1.13 g, 4 mmol), and 1-octadecene (14 g) were combined in a 50 mL three-neck round bottom flask and stirred under vacuum at 100 °C for 1 hr, then placed under a nitrogen atmosphere. Simultaneously, bis(trimethylsilyl) sulfide (TMS) (0.211 mL, 1 mmol) and 1-octadecene (4 g) were combined in a 25 mL two-neck pear-shaped flask and degassed. The TMS mixture was injected rapidly into the Pb(oleate)<sub>2</sub> solution at 85 °C and the reaction was allowed to proceed for 1.5 min, during which time the solution turned dark brown. The reaction vessel was removed from the heating mantle and was quenched by injection into 20 mL of acetone. The QD mixture was divided among centrifuge tubes and centrifuged at 8500 rpm for 10 min. After decanting the supernatant, the QDs were resuspended in minimal pentane and precipitated by centrifugation with 8 mL of acetone four more times. The PbS QDs were isolated by solvent evaporation, suspended in benzene- $d_6$ , and stored under air in the dark. The first excitonic absorbance of the HS-PbS QDs was centered at 869 nm, corresponding to a diameter of 2.78 nm as determined by the sizing curve from Moreels et al.<sup>21</sup>

**Sample preparation for <sup>1</sup>H NMR titrations.** The <sup>1</sup>H NMR samples were prepared by modifying the procedure used by Knauf et al.<sup>18</sup> An aliquot of PbS QD stock solution was removed and diluted with benzene; the concentration of the diluted aliquot was determined from the absorbance at 400 nm, using published size-dependent extinction coefficients ( $\epsilon_{400, \text{O-PbS}} = 6.61 \cdot 10^5 \text{ M}^{-1} \text{ cm}^{-1}$ ,  $\epsilon_{400, \text{HS-PbS}} = 5.01 \cdot 10^5 \text{ M}^{-1} \text{ cm}^{-1}$ ).<sup>21</sup> 50  $\mu\text{M}$  samples of QDs were prepared from the stock solution in 0.6 mL benzene- $d_6$ . 10  $\mu\text{L}$  of a ferrocene standard solution (prepared with ca. 10 mg ferrocene and 1.0 mL benzene- $d_6$ ) was added to each NMR sample as an internal standard. Stock solutions of UDA in benzene- $d_6$  (a 10  $\mu\text{L}$  volume corresponded to either 20 or 50 equivalents of UDA per QD) were titrated into the PbS QD samples.

**Sample preparation for XPS analysis.** XPS was utilized to quantify the nanocrystal stoichiometry. Samples of as-synthesized PbS QDs were prepared by drop-casting dilute solutions of QDs suspended in benzene or pentane onto Au-coated silicon wafers. Preparation of samples after exchange with UDA was as follows: 1000 equivalents of UDA (per QD) was added to a 50  $\mu\text{M}$  solution of PbS QDs in toluene and stirred for 30 min. The solution was centrifuged using acetone antisolvent, and the supernatant was decanted. An additional centrifugation step with acetone was completed after resuspension in minimal pentane and the supernatant discarded. <sup>1</sup>H NMR spectroscopy was used to confirm that no free OA or

free UDA was present in the QD sample before a diluted UDA-exchanged PbS QD solution was drop-cast onto Au-coated silicon wafers for XPS analysis.

**Sample preparation for UV-Vis and photoluminescence titrations.** An aliquot of PbS QD stock solution was diluted to ca. 5  $\mu\text{M}$  in benzene in a 1 cm path length quartz cuvette and the concentration exactly determined from the absorbance at 400 nm.<sup>21</sup> UDA was added in 20–60 equivalent intervals (a 10  $\mu\text{L}$  volume corresponded to either 20 or 50 equivalents of UDA per QD), and the absorbance spectrum was recorded after each addition. The intensity of each absorbance and photoluminescence spectrum was corrected with a dilution factor.

## Results and discussion

### Preparation and characterization of oleate-capped PbS QDs

Oleate-capped PbS QDs were synthesized via two common methods in order to assess the generality of our results. Synthetic procedures were adapted from Owen and coworkers (O-PbS)<sup>20</sup> and Hines and Scholes (HS-PbS)<sup>22</sup> to yield PbS QDs with diameters of 3.05 and 2.78 nm, respectively (Figures S1–S2). Alcohols were not employed during purification as they are known to displace X-type<sup>12</sup> and Z-type<sup>14</sup> ligands.

For both samples, the oleate (OA<sup>−</sup>) ligand density was quantified via <sup>1</sup>H NMR spectroscopy. A diagnostic broad resonance at  $\delta$  5.71 corresponds to the alkenyl protons of the bound oleate ligand (Scheme 1, H<sub>a1</sub>, H<sub>a2</sub>). The broad oleate peak is asymmetric in both sets of QDs, with a shoulder arising from a second peak centered at ca.  $\delta$  5.62 (Figures S3–S4). We attribute this peak to a small amount of residual oleic acid. The broadness of this peak as well as the observed downfield shift compared to the isolated oleic acid (OA) resonance ( $\delta$  5.49) suggests that this subpopulation is not freely diffusing throughout the solution and may be weakly associated with the ligand shell and/or engaged in rapid exchange with the bound ligands.<sup>23,24</sup>

PbS QD concentration was determined via UV-Vis absorbance spectroscopy using the size-dependent extinction coefficient at 400 nm.<sup>21</sup> Using the density of bound ligands from <sup>1</sup>H NMR spectra and QD concentration, the native oleate ligand density was determined to be  $2.87 \pm 0.23$  oleates/nm<sup>2</sup> for 50  $\mu\text{M}$  solutions of O-PbS QDs and  $2.92 \pm 0.32$  oleates/nm<sup>2</sup> for 50  $\mu\text{M}$  solutions of HS-PbS QDs (Table S1). For comparison, Weiss and coworkers have reported ligand densities of 6.7 oleates/nm<sup>2</sup> for 3.2 nm PbS QDs prepared via the method of Hines and Scholes<sup>25</sup> and Owen and coworkers have reported ligand densities of 5.7 oleates/nm<sup>2</sup> and 2.9 oleates/nm<sup>2</sup> for 3.4 nm and 6.5 nm O-PbS QDs, respectively<sup>20</sup> (Table S2). The large range of ligand coverages reported in the literature likely reflects variation in purification procedures.

To evaluate whether ligand coverage changes could be due to absolute QD concentration, the effect of dilution upon oleate density was studied.<sup>26</sup> Upon dilution of 100  $\mu\text{M}$  QD solutions, the ligand density remained the same within error for both sets of QDs (Table S3). From these data, we expect the ligand shell

density to remain constant and only change in composition during our ligand exchange titrations.

### Probing the mechanism of ligand exchange

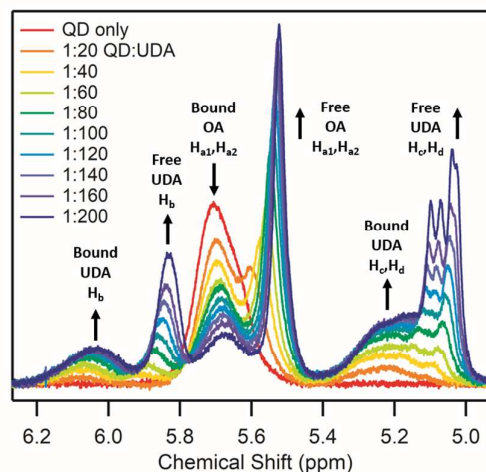
Ligand exchange reactions between the native oleate ligands and undec-10-enoic acid (UDA) were quantified for O-PbS and HS-PbS QDs. The  $^1\text{H}$  NMR signals for both freely diffusing and QD-bound forms of oleic acid and UDA can be distinguished by their unique chemical shifts, relative broadness, and splitting patterns, allowing for quantification of the surface ligand exchange reaction using the integration of these distinct resonances.<sup>18</sup> To account for the residual unbound oleic acid in the isolated QDs, the moles of free oleic acid present in the absence of UDA were subtracted from the total moles of free OA in each subsequent spectrum. The concentrations of OA and UDA were quantified by integration of the respective peaks versus the integration of the ferrocene resonance in the  $^1\text{H}$  NMR spectra (see Figure S5 for example integration). While peaks corresponding to  $\text{H}_c$  and  $\text{H}_d$  have distinct chemical shifts in the spectrum of isolated UDA, these features are integrated together as they cannot be deconvoluted in our NMR titrations due to peak broadening.

Titration of UDA in aliquots of 20–100 equivalents provides insight into the ligand shell composition at each point in the titration with the growth of signals for free OA ( $\text{H}_{a1}, \text{H}_{a2}$ ,  $\delta$  5.51) and the concomitant loss of the bound  $\text{OA}^-$  ( $\text{H}_{a1}, \text{H}_{a2}$ ,  $\delta$  5.71) feature. Peaks for both freely diffusing UDA ( $\text{H}_b$ ,  $\delta$  5.81;  $\text{H}_c, \text{H}_d$ ,  $\delta$  5.04) and bound UDA ( $\text{H}_b$ ,  $\delta$  6.01;  $\text{H}_c, \text{H}_d$ ,  $\delta$  5.17) increase in intensity during the course of the titrations (Figure 1, Figure S6).

The alkene resonance of isolated OA in benzene- $d_6$  is an overlapping doublet of triplets centered at  $\delta$  5.49 ( $\text{H}_{a1}, \text{H}_{a2}$ ). The vinylic resonances of isolated UDA in benzene- $d_6$  are multiplets centered at  $\delta$  5.03 ( $\text{H}_b$ ) and ca.  $\delta$  5.79 ( $\text{H}_c, \text{H}_d$ ). However, upon titration of UDA into PbS QDs, the  $^1\text{H}$  NMR signals for free OA and free UDA retain broadness through 200 equivalents of UDA (Figure 1), suggesting a dynamic exchange equilibrium between the free and bound populations through an entangled, physisorbed intermediate.<sup>23</sup> Peak broadness can in part be attributed to the rapid transversal relaxation of molecules with restricted rotational degrees of freedom, yet broadness also signifies exchange processes between ligands. A dynamic exchange is further consistent with the gradual upfield shift of the free peaks over the course of the titration, caused by the increase in concentration of free ligand that does not interact with the QD ligand shell. Upon addition of  $\geq 500$  equivalents of UDA, the splitting and resolution of the free OA resonance approach that of the isolated OA resonance, which suggests that the mole fraction of OA freely diffusing in solution is greater than the fraction of free ligand entangled within the ligand shell (Figure S7).<sup>23</sup>

The exchange ratio between bound UDA and free OA, as quantified by  $^1\text{H}$  NMR integration, remains approximately 1:1 across all concentrations of UDA. The total ligand coverage remains constant throughout the titration, which is further in agreement with a 1:1 exchange (Tables S4-S5). The near unity

exchange ratio between free OA and bound UDA ( $1:1.21 \pm 0.17$  for O-PbS and  $1:1.08 \pm 0.15$  for HS-PbS) and constant total ligand coverage is consistent with an X-type exchange



mechanism wherein each UDA ligand displaces one native

**Fig. 1**  $^1\text{H}$  NMR spectra of 50  $\mu\text{M}$  O-PbS QDs (3.05 nm) titrated with undec-10-enoic acid (UDA) in benzene- $d_6$ .

oleate and does not support a primary reaction pathway in which UDA initially binds to uncoordinated surface lead atom (see below for further discussion).<sup>17,23</sup> This stoichiometric exchange mechanism matches that observed for the identical ligand exchange process involving CdSe QDs<sup>18</sup> and between *trans*-2,6-difluorocinnamic acid and OA for O-PbS QDs<sup>17</sup>.

While the  $^1\text{H}$  NMR data are highly suggestive that an X-type reaction is the dominant exchange mechanism, additional spectroscopic characterization is required to definitively distinguish between metal carboxylate liberation in Z-type ligand displacements and carboxylic acid release in pure X-type exchange reactions. Although inductively-coupled plasma mass spectrometry (ICP-MS) is regularly employed to assess metal:chalcogenide ratios of QDs, quantification of the Pb:S ratio by ICP-MS is known to be inaccurate, as digestion of sulfides with nitric acid leads to the formation of volatile  $\text{H}_2\text{S}$ .<sup>21</sup> XPS provides an alternate means of determining the inorganic composition of QDs and is suitable for sulfur-containing QDs.<sup>6,27–29</sup> Pb:S ratios before and after the addition of 1000 equivalents of UDA (Figures S8-S9) are the same within error for both sets of nanocrystals (Table 1). This is inconsistent with a Z-type mechanism in which  $\text{Pb}(\text{carboxylate})_2$  ligands would be displaced from the surface, further supporting a majority X-type ligand exchange mechanism. The Pb:S ratios for as-synthesized QDs are also in agreement with literature values (Table 2, see SI for theoretical Pb:S ratio calculations).

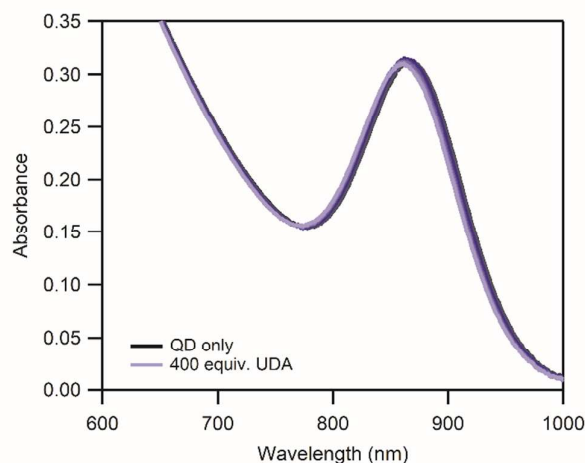
**Table 1** Pb:S ratios determined via XPS before and after exchange with UDA.

Sample	as-synthesized	after UDA exchange
O-PbS	$1.81 \pm 0.06$	$1.83 \pm 0.10$
HS-PbS	$1.91 \pm 0.09$	$1.84 \pm 0.03$

**Table 2** Previously reported Pb:S ratios quantified via XPS.

Method of synthesis	Diameter (nm)	Pb:S ratio	Ref
Owen	3.2	2.26	27
Hines-Scholes	2.9	1.75	28
Hines-Scholes	2.9	1.55 ± 0.07	6

To further evaluate how ligand exchange impacts the surface electronic structure of the inorganic core, the excitonic transition was monitored via UV-Visible absorbance spectroscopy during UDA titrations. Absorbance features are sensitive to changes in the surface ligands due to coupling of the electronic structure of the surface with the exciton confined within the core.<sup>30</sup> Increasing UDA concentrations up to 400 equivalents resulted in 7 and 10 nm blue shifts in the excitonic features for HS-PbS (Figure 2) and for O-PbS (Figure S10), respectively. While blue shifts of absorbance features can indicate a change in the nanocrystal core size due to etching of the surface,<sup>31</sup> the small hypsochromic shifts observed here correspond to less than 1 lattice unit reduction in size (Table S6) and are likely due to a decrease in solvent shielding resulting from the shorter UDA ligand rather than surface etching. This conclusion is further supported by the invariant Pb:S ratio before and after UDA addition as well as the preservation of 90% of the excitonic emission (Figure S11).

**Fig. 2** UV-Visible absorption titration of 400 equivalents of undec-10-enoic acid (UDA) to 4.75 μM HS-PbS QDs in benzene.

### Quantification of ligand exchange processes

The stoichiometric 1:1 ligand exchange established by <sup>1</sup>H NMR and XPS measurements allows an equilibrium constant for the ligand exchange reaction (Eq. 1) to be calculated. The equilibrium constant ( $K_{eq}$ ) is determined from Equation 2



$$K_{eq} = \frac{[\text{OA}]_F [\text{UDA}^-]_B}{[\text{OA}^-]_B [\text{UDA}]_F} \quad (2)$$

where  $[\text{OA}^-]_B$  is the concentration of bound OA,  $[\text{OA}]_F$  is the concentration of free OA,  $[\text{UDA}^-]_B$  is the concentration of bound UDA, and  $[\text{UDA}]_F$  is the concentration of free UDA as determined by integration of the alkenyl signals in the <sup>1</sup>H NMR spectra.

Using <sup>1</sup>H NMR data from spectra recorded with 0–600 equivalents of UDA,  $K_{eq}$  values of  $2.23 \pm 0.50$  and  $2.14 \pm 0.42$  were determined for O-PbS and HS-PbS QDs, respectively (Tables S4-S5). Agreement of these  $K_{eq}$  values indicates that these widely used synthetic techniques produce QDs with surface compositions that do not quantitatively differ in their reactivity toward the titrated UDA ligand. To verify reversibility of the exchange process, OA was added after the titration with UDA. Upon addition of UDA, the equilibrium constants (calculated with Equation 2) of  $2.30 \pm 0.40$  for O-PbS and  $1.92 \pm 0.42$  for HS-PbS (Tables S7-S8) are consistent with those quantified in the initial titration with UDA. In accordance with Le Chatelier's principle, the addition of OA increases the bound oleate signal and decreases the bound UDA peaks, supporting assignment of the exchange equilibrium process (Figure S12).

Comparing the quantitative  $K_{eq}$  values for the exchange of OA and UDA on PbS QDs to those of other systems affords deeper understanding of how ligand structure influences the exchange process. Beard and coworkers recently evaluated a cooperative exchange process between native oleate ligands and *trans*-2,6-difluorocinnamic acid on O-PbS QDs.<sup>17</sup> In this system, the  $K_{eq}$  value increased as the coverage of *trans*-2,6-difluorocinnamic acid increased. This behavior was ascribed to the ability of the fluorinated aryl tails to engage in  $\pi$ - $\pi$  stacking – a favorable ligand–ligand interaction that can promote subsequent ligand addition. However, the short, fluorinated aryl tails of *trans*-2,6-difluorocinnamic acid are substantially different than the long aliphatic tails of OA and UDA. The equilibrium constant for the exchange of OA and UDA was not found to depend on the concentration of UDA, which is an expected result given the weak ligand–ligand interactions and lack of  $\pi$ - $\pi$  stacking electronic effects between the aliphatic chains of OA and UDA.

The impact of the core material on ligand exchange can be elucidated by quantitative evaluation of the same exchange reaction for a series of inorganic core materials. The  $K_{eq}$  values for PbS QDs are greater than 1, indicating that the binding of UDA to the PbS QD surface is more favorable than the binding of OA. The carboxylate anchoring groups bound to the surface metal atoms are identical for both partners in this X-type exchange reaction making it unlikely that the identity of the anchoring groups plays a role in dictating ligand binding, though the structure of the exchanging ligand chains could still influence ligand affinity for the surface. Interestingly, comparison of this data to the  $K_{eq}$  for the identical exchange reaction on 2.9 nm CdSe QDs paints a more complex picture. Investigations of CdSe QDs yielded a  $K_{eq}$  less than 1 ( $K_{eq} = 0.84 \pm 0.05$ ) that is constant across UDA concentrations, indicating that binding of OA to the QD surface is favored.<sup>18</sup> However, the steric interactions between the ligand chains of UDA and OA cannot exclusively control the affinity of ligands

for the nanocrystal surface, otherwise comparable  $K_{\text{eq}}$  values for each semiconductor material would be expected. QD size and solvent effects are also unlikely explanations for the observed difference in ligand affinity between these materials as the QDs employed in these two studies are approximately the same diameter and the ligand exchanges were analyzed in similar solvents (benzene for PbS, toluene for CdSe). While ligand coverage differed between the PbS (2.9 oleates/nm<sup>2</sup>) and CdSe (1.4 oleates/nm<sup>2</sup>) QDs studied in our lab, Hens and coworkers found a nearly identical  $K_{\text{eq}}$  value for CdSe with substantially higher ligand coverage (3.2 oleates/nm<sup>2</sup>),<sup>19</sup> suggesting that tighter packing alone does not dictate the relative  $K_{\text{eq}}$ . For these reasons, we hypothesize that the composition of the surface crystal facets influences the relative  $K_{\text{eq}}$  values for PbS and CdSe.

Computational models of rock salt PbS QDs<sup>32</sup> and zinc blende CdSe QDs<sup>33</sup> have revealed eight {111} facets and six {100} facets for each material, yet the metal chalcogenide composition of these facets differs for each semiconductor due to the underlying crystal structure. For PbS, the neutral (001) facet is a checkerboard pattern of lead and sulfur atoms which does not require X-type oleates for charge balance.<sup>32</sup> The (111) facet can be either lead- or sulfur-rich; a lead-rich surface would require X-type ligands for charge balance while a sulfur-rich surface could host Z-type Pb(oleate)<sub>2</sub> species. Both scenarios would lead to a cation-rich QD, as is generally observed for PbS (Table 2) and CdSe. By contrast, the (100) and (111) facets of CdSe can each expose either cadmium or selenium ions.<sup>16</sup> The differences between the available facets—and the boundaries between them—may underpin nuanced ligand-ligand interactions and ligand packing arrangements related to the intrinsically straight structure of UDA vs. the “kinked” oleate ligand that influence the observed  $K_{\text{eq}}$ .

The slight deviation from a strict 1:1 exchange ratio observed for PbS (Tables S4-S5) may also explain the difference in the  $K_{\text{eq}}$  values for PbS and CdSe, as it suggests a binding affinity for neutral UDA on PbS. Binding of carboxylic acid as a neutral ligand has been reported to be energetically favorable for the (001) facet of PbS, albeit with a substantially weaker binding energy than an X-type ligand bound to a cation-rich surface.<sup>32</sup> The (001) facet is likely uncoordinated after the extensive purification procedures employed, so UDA may associate as a neutral ligand during the course of the titration, contributing to the higher effective  $K_{\text{eq}}$  values for this material. Together, these data highlight the subtleties of ligand exchange reactions and QD surfaces and underscore the need to improve quantification and insight into these complex processes.

## Conclusions

The mechanism of ligand exchange between carboxylate-terminated oleate and UDA ligands was evaluated for PbS QDs synthesized via two distinct routes. <sup>1</sup>H NMR spectroscopy was used to quantify the exchange equilibrium of this reaction and yielded a similar equilibrium constant for both sets of PbS QDs ( $K_{\text{eq}} = 2.23 \pm 0.50$  and  $2.14 \pm 0.42$  for O-PbS and HS-PbS, respectively), demonstrating that the surface chemistry of each

set of QDs is indistinguishable. XPS and optical spectroscopies were employed to conclude that Z-type ligand dissociation or displacement did not occur, and that the dominant pathway was an X-type exchange mechanism. This study illustrates the dependence of ligand exchange reactions on ligand structure and semiconductor material, which can dictate the binding and packing of native and exchange ligands on the crystal facets. The quantification of this aliphatic carboxylate-carboxylate exchange will contribute to a deeper understanding of complex ligand exchange reactions.

## Conflicts of interest

The authors declare no competing financial interest.

## Acknowledgements

This material is based upon work supported by the Air Force Office of Scientific Research under AFOSR Award No. FA9550-15-1-0227 and AFOSR Award No. FA9550-16-1-0206. H.E.S. acknowledges support from the Materials Interdisciplinary Research Team funded by the National Science Foundation under grant number DMR-1436201 and a Summer Undergraduate Research Fellowship from the University of North Carolina at Chapel Hill. R.R.K. acknowledges a dissertation completion fellowship supported by The Graduate School of The University of North Carolina at Chapel Hill. K.J.R. acknowledges support from the National Science Foundation Graduate Research Fellowship Program. We thank Dr. Marc ter Horst for <sup>1</sup>H NMR assistance, Dr. Carrie Donley and Catherine McKenas for XPS measurements and Dr. Amar S. Kumbhar for TEM measurements at CHANL, and Dr. Kyle Brennaman for assistance with the photoluminescence spectrometer. This work made use of Cary 50 UV-Visible absorbance spectrophotometer and PTI QuantaMaster 4SE-NIR emission spectrophotometer instruments in the UNC EFRC Instrumentation Facility established by the UNC EFRC: Center for Solar Fuels, an Energy Frontier Research Center funded by the U.S. Department of Energy, Office of Science, Office of Basic Energy Sciences under Award Number DE-SC0001011. This work was performed in part at the Chapel Hill Analytical and Nanofabrication Laboratory, CHANL, a member of the North Carolina Research Triangle Nanotechnology Network, RTNN, which is supported by the National Science Foundation, Grant ECCS-1542015, as part of the National Nanotechnology Coordinated Infrastructure, NNCI.

## Notes and references

- 1 N. Zhao, T. P. Osedach, L.-Y. Chang, S. M. Geyer, D. Wanger, M. T. Binda, A. C. Arango, M. G. Bawendi and V. Bulovic, *ACS Nano*, 2010, **4**, 3743–3752.
- 2 Y. Hara, A. Gadisa, Y. Fu, T. Garvey, K. T. Vroouwenvelder, C. W. Miller, J. L. Dempsey and R. Lopez, *J. Phys. Chem. C*, 2016, **120**, 8005–8013.

- 3 G. H. Carey, A. L. Abdelhady, Z. Ning, S. M. Thon, O. M. Bakr and E. H. Sargent, *Chem. Rev.*, 2015, **115**, 12732–12763.
- 4 B. A. Kairdolf, A. M. Smith, T. H. Stokes, M. D. Wang, A. N. Young and S. Nie, *Annu. Rev. Anal. Chem.*, 2013, **6**, 143–62.
- 5 Y. Yin and A. P. Alivisatos, *Nature*, 2005, **437**, 664–670.
- 6 A. Shestha, Y. Yin, G. G. Andersson, N. A. Spooner, S. Qiao and S. Dai, *Small*, 2017, **13**, 1602956.
- 7 C. C. Reinhart and E. Johansson, *Chem. Mater.*, 2015, **27**, 7313–7320.
- 8 K.-R. Lee, S. Bettis Homan, M. Kodaimati, G. C. Schatz and E. A. Weiss, *J. Phys. Chem. C*, 2016, **120**, 22186–22194.
- 9 C. Giansante, I. Infante, E. Fabiano, R. Grisorio, G. P. Suranna and G. Gigli, *J. Am. Chem. Soc.*, 2015, **137**, 1875–1886.
- 10 E. Cohen, P. Komm, N. Rosenthal-Strauss, J. Dehnel, E. Lifshitz, S. Yochelis, R. D. Levine, F. Remacle, B. Fresch, G. Marcus and Y. Paltiel, *J. Phys. Chem. C*, 2018, **122**, 5753–5758.
- 11 N. C. Anderson and J. S. Owen, *Chem. Mater.*, 2013, **25**, 69–76.
- 12 A. Hassinen, I. Moreels, K. De Nolf, P. F. Smet, J. C. Martins and Z. Hens, *J. Am. Chem. Soc.*, 2012, **134**, 20705–20712.
- 13 R. Gomes, A. Hassinen, A. Szczygiel, Q. Zhao, A. Vantomme, J. C. Martins and Z. Hens, *J. Phys. Chem. Lett.*, 2011, **2**, 145–152.
- 14 N. C. Anderson, M. P. Hendricks, J. J. Choi and J. S. Owen, *J. Am. Chem. Soc.*, 2013, **135**, 18536–18548.
- 15 E. Drijvers, J. De Roo, J. C. Martins, I. Infante and Z. Hens, *Chem. Mater.*, 2018, **30**, 1178–1186.
- 16 M. Saniepay, C. Mi, Z. Liu, E. P. Abel and R. Beaulac, *J. Am. Chem. Soc.*, 2018, **140**, 1725–1736.
- 17 D. M. Kroupa, N. C. Anderson, C. V. Castaneda, A. J. Nozik and M. C. Beard, *Chem. Commun.*, 2016, **52**, 13893–13896.
- 18 R. R. Knauf, J. C. Lennox and J. L. Dempsey, *Chem. Mater.*, 2016, **28**, 4762–4770.
- 19 K. De Nolf, S. M. Cosseddu, J. J. Jasieniak, E. Drijvers, J. C. Martins, I. Infante and Z. Hens, *J. Am. Chem. Soc.*, 2017, **139**, 3456–3464.
- 20 M. P. Hendricks, M. P. Campos, G. T. Cleveland, I. Jen-La Plante and J. S. Owen, *Science*, 2015, **348**, 1226–1230.
- 21 I. Moreels, K. Lambert, D. Smeets, D. De Muynck, T. Nollet, J. C. Martins, F. Vanhaecke, A. Vantomme, C. Delerue, G. Allan and Z. Hens, *ACS Nano*, 2009, **3**, 3023–3030.
- 22 M. a. Hines and G. D. Scholes, *Adv. Mater.*, 2003, **15**, 1844–1849.
- 23 B. Fritzing, R. K. Capek, K. Lambert, J. C. Martins and Z. Hens, *J. Am. Chem. Soc.*, 2010, **132**, 10195–10201.
- 24 Z. Hens and J. C. Martins, *Chem. Mater.*, 2013, **25**, 1211–1221.
- 25 C. He, D. J. Weinberg, A. B. Nepomnyashchii, S. Lian and E. A. Weiss, *J. Am. Chem. Soc.*, 2016, jacs.6b03970.
- 26 A. B. Nepomnyashchii, R. D. Harris and E. A. Weiss, *Anal. Chem.*, 2016, **88**, 3310–3316.
- 27 D. M. Kroupa, M. Vörös, N. P. Brawand, B. W. McNichols, E. M. Miller, J. Gu, A. J. Nozik, A. Sellinger, G. Galli and M. C. Beard, *Nat. Commun.*, 2017, **8**, 15257.
- 28 B. Hou, Y. Cho, B. S. Kim, J. Hong, J. B. Park, S. J. Ahn, J. I. Sohn, S. Cha and J. M. Kim, *ACS Energy Lett.*, 2016, **1**, 834–839.
- 29 E. M. Miller, D. M. Kroupa, J. Zhang, P. Schulz, A. R. Marshall, A. Kahn, S. Lany, J. M. Luther, M. C. Beard, C. L. Perkins and J. Van De Lagemaat, *ACS Nano*, 2016, **10**, 3302–3311.
- 30 M. Krause and P. Kambhampati, *Phys. Chem. Chem. Phys.*, DOI:10.1039/C5CP02173A.
- 31 M. T. Frederick, V. a Amin, L. C. Cass and E. A. Weiss, *Nano Lett.*, 2011, **11**, 5455–60.
- 32 D. Zhrebetsky, M. Scheele, Y. Zhang, N. Bronstein, C. Thompson, D. Britt, M. Salmeron, P. Alivisatos and L.-W. Wang, *Science*, 2014, **344**, 1380–1384.
- 33 A. J. Houtepen, Z. Hens, J. S. Owen and I. Infante, *Chem. Mater.*, 2017, **29**, 752–761.